Spatial correlation vortices in partially coherent light: theory

Ivan D. Maleev, David M. Palacios, Arvind S. Marathay, and Grover A. Swartzlander, Jr.

Optical Sciences Center, University of Arizona, Tucson, Arizona 85721

Received February 19, 2004; revised manuscript received June 11, 2004

Spatial correlation vortex dipoles may form in the four-dimensional mutual coherence function when a partially coherent light source contains an optical vortex. Analytical and numerical investigations are made in near- and far-field regimes. © 2004 Optical Society of America

OCIS codes: 030.1640, 030.1670, 100.4550, 260.0260, 350.5030.

1. INTRODUCTION

Coherent optical beams may contain optical vortices that are characterized by a dark core and a well-defined azimuthally harmonic phase.[1,2] In contrast, different points in a spatially incoherent beam are uncorrelated, and the phase structure of an optical vortex is ill defined. In the transitional regime of partially coherent light, one should take the statistical properties of light into account to quantify global phase properties.[3,4] Recent investigations suggest that vortices in partially coherent light are destroyed.[5,6] By relating the vortex phase to the spatial variations in the mutual coherence function[4] (MCF), we found robust vortex attributes that do not vanish in partially coherent light.

The coherence properties of optical vortices have become an active branch of inquiry in singular optics over the past several years. Coherence filtering properties of an optical vortex were recently investigated numerically[7] and experimentally.[8] We employed the MCF, which describes the correlation between two points in a beam, to study the propagation of partially coherent beams.[9] Recently the MCF was used to study phase singularities in partially coherent light emerging from two pinholes[10,11] and to analyze sources with separable phase.[12]

Here we describe our numerical investigation of the MCF of a partially coherent vortex beam. We found spatial correlation vortices (SCVs) in the MCF, which are analogous to the composite vortices in coherent beams.[2,13] Furthermore we demonstrate how both the coherence length and the displacement of the conventional vortex in a beam affect the SCVs. An on-axis vortex in a partially coherent beam may result in a circular dislocation line in the MCF.[14] We found that this dislocation breaks into two spatial correlation vortices as the conventional vortex is moved off axis.

2. OPTICAL VORTEX IN THE INITIAL PLANE

A single optical vortex in a coherent scalar beam that has an otherwise planar wave front may be represented by the complex electric field in the initial transverse plane ($z = 0$) (Refs. 2 and 13):

$$E(r,\ \phi,\ t) = A(r')g(r)\exp(im\phi')\exp(i\omega t)\exp(i\beta), \tag{1}$$

where the transverse polar coordinates $(r,\ \phi)$ and $(r',\ \phi')$ are measured with respect to the center of the beam and to the vortex core, respectively (see Fig. 1), ω is the angular frequency, t is the time, m is the topological charge, and β is an arbitrary phase. We assume that the beam envelope, $g(r)$, is radially symmetric about the beam center $(r = 0)$ and has a characteristic size w_0. Furthermore, we assume that the vortex core function, $A(r')$, is symmetric about the vortex core $(r' = 0)$. The vectors $\mathbf{r}$ and $\mathbf{r}'$ are related by displacement vector $\mathbf{s}$: $\mathbf{r} = \mathbf{r}' + \mathbf{s}$. If the vortex core coincides with the beam center $(s = 0)$, we refer to an on-axis vortex; otherwise $(s \neq 0)$ the beam is said to contain an off-axis vortex. Intensity and phase profiles of an off-axis vortex are depicted in Figs. 1(a) and 1(b), respectively. When m is a nonzero integer the field described by Eq. (1) has an undefined phase at $\mathbf{r}' = 0$; hence the field there must vanish. Physically this zero-field point is attributed to total destructive interference.

In this paper we discuss two types of initial vortex core profile: large-core and pointlike profiles. Large-core vortices, which occur naturally in laser modes and speckle, have a core function that may be expressed as $A(r') = (r'/w_0)^{|m|}$. "Large" refers to the fact that the core function has infinite extent; the effective core size is limited by envelope function $g(r)$. We note that when $s = 0$ a large-core vortex and a Gaussian envelope function represent a Laguerre–Gaussian mode. Pointlike vortices have a localized core that may be approximated by $A(r') = \tanh^{|m|}(r'/b)$, assuming that the radial core size, b, is much smaller than the envelope size, w_0.[2,15,16] Producing pointlike vortices requires diffractive masks or holograms. For example, one may create a point vortex by transmitting a planar Gaussian beam $(m = 0)$ through a phase mask of variable thickness $d = d_0 - m\lambda_0\phi/2\pi(n_s - n_0)$, where d_0 is the maximum thickness, λ_0 is the intended wavelength, and n_s and n_0 are indices of refraction of the substrate and of the surrounding medium, respectively.[16,17]

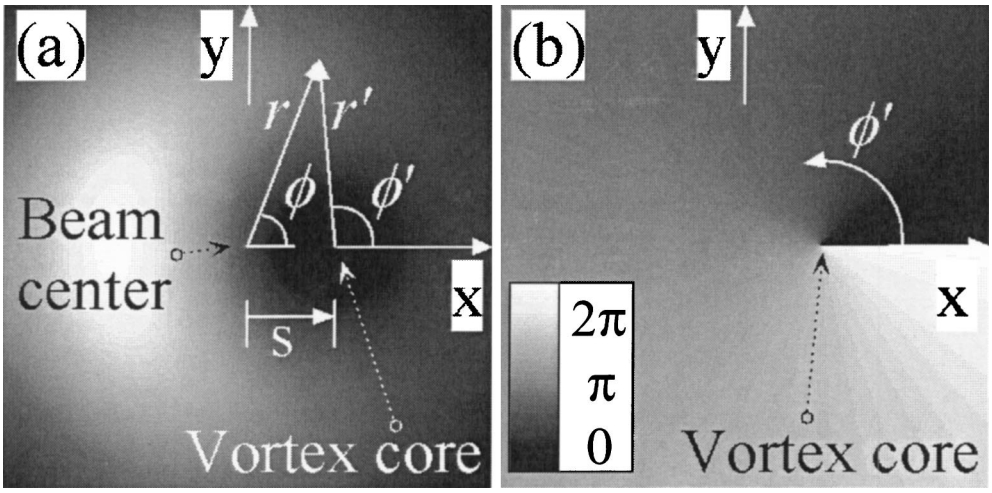

Fig. 1. Initial (a) intensity and (b) phase profiles of an electromagnetic field vortex of topological charge $m = 1$. Vector $\mathbf{s}$ shows the displacement of the vortex core from the centroid of the beam envelope. Position vectors $\mathbf{r}$ and $\mathbf{r}'$, respectively, make angles ϕ and ϕ' with the x axis and are related: $\mathbf{r} = \mathbf{r}' + \mathbf{s}$. When $m = 1$ the vortex phase is equivalent to angle ϕ'.

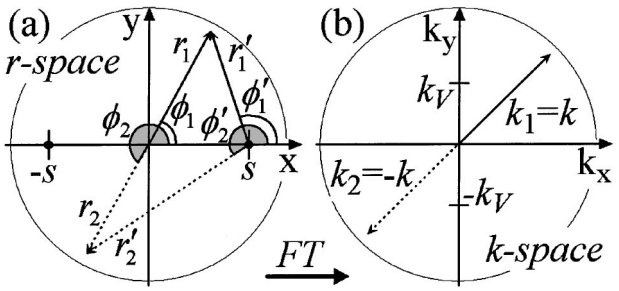

Fig. 2. Notation used to describe the mutual coherence function in the (a) initial and (b) far-field planes. Unprimed (primed) variables are measured from the beam envelope (vortex) center. FT, Fourier transform.

3. MUTUAL COHERENCE FUNCTION IN THE INITIAL PLANE

A partially coherent beam propagating through a vortex mask may be expected to gain the characteristic vortex phase factor $\exp(im\phi')$ even though the wave front is randomized. We may formalize this assertion by interpreting the phase β in Eq. (1) as a spatially distributed random variable. For computational convenience we assume that the statistical distribution of β corresponds to a Schell-model correlator: $C(\mathbf{r}_1, \mathbf{r}_2) = C(|\mathbf{r}_1 - \mathbf{r}_2|)$, where $C(0) = 1$ and $\mathbf{r}_1$ and $\mathbf{r}_2$ are arbitrary points in the initial plane (see Fig. 2). Coherence properties of a statistically stationary field may be described by the MCF:

$$\Gamma(\mathbf{r}_1, \mathbf{r}_2) = \langle E(\mathbf{r}_1, t)E^*(\mathbf{r}_2, t)\rangle, \tag{2}$$

where $\langle\ \rangle$ denotes an ensemble average. The MCF for a partially coherent vortex field may therefore be expressed by insertion of Eq. (1) into Eq. (2):

$$\Gamma(\mathbf{r}_1, \mathbf{r}_2) = C(\mathbf{r}_1 - \mathbf{r}_2)A(r_1')A(r_2')g(r_1)g(r_2) \times \exp[im(\phi_1' - \phi_2')], \tag{3}$$

where $\mathbf{r}_1 = \mathbf{r}_1' + \mathbf{s}$ and $\mathbf{r}_2 = \mathbf{r}_2' + \mathbf{s}$. Equation (3) may be understood as a four-dimensional field containing two vortices that have topological charges $+m$ and $-m$, i.e., a vortex dipole.

The four-dimensional MCF may be partially characterized by two two-dimensional functions: intensity $I(\mathbf{r})$ and normalized cross correlation $\chi(\mathbf{r})$. The latter may be experimentally determined by use of a wave-front folding interferometer.[3] In the initial plane these functions are given by

$$I(\mathbf{r}) = \Gamma(\mathbf{r}, \mathbf{r}) = A^2(|\mathbf{r} - \mathbf{s}|)g^2(r), \tag{4a}$$

$$\chi(\mathbf{r}) = \Gamma(\mathbf{r}, -\mathbf{r})/[I(\mathbf{r})I(-\mathbf{r})]^{1/2} = C(2\mathbf{r})\exp(im\Phi), \tag{4b}$$

where $\exp(i\Phi) = \exp[i(\phi_1' - \phi_2')] = -[r^2 - s^2 + 2i(ys_x - xs_y)]/(|\mathbf{r} - \mathbf{s}||\mathbf{r} + \mathbf{s}|)$ and where (x, y) and (s_x, s_y) are the Cartesian coordinates of vectors $\mathbf{r}$ and $\mathbf{s}$, respectively. The intensity at the origin, $I(0) = A^2(s)g^2(0)$, is equal to zero when $s = 0$. The phase, Φ, is undefined at the singularities located at $\mathbf{r} = \pm\mathbf{s}$. Furthermore, we note that $\exp(i\Phi) = +1$ at $r = 0\ (s \neq 0)$ and $\exp(i\Phi) = -1$ when $s = 0\ (r \neq 0)$.

Thus in the initial plane a single dark core appears in the intensity profile at $\mathbf{r} = \mathbf{s}$ [as shown in Fig. 1(a)], and two oppositely charged phase singularities, or correlation vortices, appear at $\mathbf{r} = \pm\mathbf{s}$. The magnitude of $\chi(\mathbf{r})$ is given by correlator $C(2\mathbf{r})$ at all points except the singularities, where $|\chi(\pm\mathbf{s})|$ must abruptly vanish because Φ is undefined at $\mathbf{r} = \pm\mathbf{s}$. The distance over which the value of $|\chi|$ changes from $C(2\mathbf{r})$ to zero is negligible. Each near-field normalized cross-correlation vortex may therefore be categorized as a point vortex in the initial plane. Experimentally these correlation vortices may be manifest as points of zero fringe visibility in the measured output of a wave-front folding interferometer. When $s = 0$ the correlation vortices are annihilated and we find that $\chi(\mathbf{r}) = (-1)^m C(2\mathbf{r})$ (except at the origin). We also see that when $s = 0$ the beam uniformly switches between correlation and anti-correlation values when the value of m is changed from even to odd. This result reflects the fact that the points at $\mathbf{r}$ and $-\mathbf{r}$ are in (out of) phase when m is even (odd). These results, which follow from Eqs. (4), are independent of the explicit forms of the vortex core function, the amplitude function, and the correlator.

4. FAR FIELD MUTUAL COHERENCE FUNCTION

Both the optical field and the MCF change as the beam propagates through free space. This change is most easily understood for the far-field regime (i.e., at a propagation distance $z_d \gg k{w_0}^2$), where both large-core and point vortices in the initial plane are transformed into large-core vortices when the beam is coherent.[2,15,16] Lacking *a priori* knowledge of the far-field correlator, one may calculate the MCF from Eq. (3) (Ref. 3):

$$\Gamma^{\infty}(\mathbf{k}_1, \mathbf{k}_2) = (1/\lambda z_d)^2 \int\int \Gamma(\mathbf{r}_1, \mathbf{r}_2)\exp[-i(\mathbf{k}_1\cdot\mathbf{r}_1 - \mathbf{k}_2\cdot\mathbf{r}_2)]\mathrm{d}\mathbf{r}_1\mathrm{d}\mathbf{r}_2, \tag{5}$$

where $\mathbf{k}_1$ and $\mathbf{k}_2$ are transverse wave vectors in the far-field plane [Fig. 2(b)]. As we did for the initial plane, we focus our attention on the far-field intensity, $I^{\infty}(\mathbf{k}) = \Gamma(\mathbf{k}, \mathbf{k})$ and on the normalized cross-correlation function, $\chi^{\infty}(\mathbf{k}) = \Gamma^{\infty}(\mathbf{k}, -\mathbf{k})/[I^{\infty}(\mathbf{k})I^{\infty}(-\mathbf{k})]^{1/2}$.

Efficient fast-Fourier-transform algorithms[18] may be used to integrate Eq. (5) numerically. Although the four-dimensional computation is generally memory intensive, it is possible to choose envelope and core functions that allow Eq. (5) to be computed from two-dimensional integrals. For this reason we assume that the optical field in the initial plane is described by a large-core vortex of topological charge $m = 1$ on a Gaussian envelope, $g(r) = E_0 \exp(-r^2/{w_0}^2)$, where E_0 and w_0 characterize the field amplitude (assumed to be real) and the radial beam size, respectively. Furthermore we assume a Gaussian–Schell correlator[4]:

$$C(\mathbf{r}_1 - \mathbf{r}_2) = \exp(-|\mathbf{r}_1 - \mathbf{r}_2|^2/{l_C}^2), \tag{6}$$

where l_C is the transverse coherence length in the initial plane. For the planar (nonvortex) case, $m = 0$, Eq. (5) reduces to $\Gamma^{\infty}_{m=0}(\mathbf{k}_1, \mathbf{k}_2) = (E_0/\lambda z_d)^2(\int\int T_x\mathrm{d}x_1\mathrm{d}x_2 \times \int\int T_y\mathrm{d}y_1\mathrm{d}y_2)$, where

$$T_x = \exp(-({x_1}^2 + {x_2}^2)/{r_{\mathrm{bs}}}^2 + 2x_1x_2/{l_C}^2) \times \exp(ik_{2x}x_2 - ik_{1x}x_1), \tag{7a}$$

$$T_y = \exp(-({y_1}^2 + {y_2}^2)/{r_{\mathrm{bs}}}^2 + 2y_1y_2/{l_C}^2) \times \exp(ik_{2y}y_2 - ik_{1y}y_1), \tag{7b}$$

where (x_i, y_i) and (k_{ix}, k_{iy}) are the coordinates of $\mathbf{r}_i$ and $\mathbf{k}_i$, respectively, and the beam spread parameter is defined $r_{\mathrm{bs}} = [(1/{w_0}^2) + (1/{l_C}^2)]^{-1/2}$.

A. On-Axis Case, $s=0$, $m=1$

It is instructive first to consider the on-axis case for a fundamental charge, $m = 1$, whereby Eq. (5) may be expressed:

$$\Gamma^{\infty}_{m=1}(\mathbf{k}_1, \mathbf{k}_2) = (E_0/w_0\lambda z_d)^2\Big(\int\int x_1x_2T_x\mathrm{d}x_1\mathrm{d}x_2 \times \int\int T_y\mathrm{d}y_1\mathrm{d}y_2 + \int\int x_1T_x\mathrm{d}x_1\mathrm{d}x_2\int\int iy_2T_y\mathrm{d}y_1\mathrm{d}y_2 + \int\int x_2T_x\mathrm{d}x_1\mathrm{d}x_2\int\int iy_1T_y\mathrm{d}y_1\mathrm{d}y_2 + \int\int T_x\mathrm{d}x_1\mathrm{d}x_2\int\int y_1y_2T_y\mathrm{d}y_1\mathrm{d}y_2\Big). \tag{8}$$

The far-field intensity, $I^{\infty}(\mathbf{k})$, and both the modulus[19] and the phase of $\chi^{\infty}(\mathbf{k})$ are shown in Fig. 3 for different values of the relative coherence length $\sigma_c = l_c/w_0$. As expected, the intensity profiles in Figs. 3(a)–3(c) depict greater diffusion of light into the vortex core as the value of σ_c decreases.

A striking dark ring, which persists as σ_c is varied, is evident in the normalized cross-correlation function shown in Figs. 3(d)–3(f). The phase profiles in Figs. 3(g)–3(i) depict a π phase difference on either side of the ring, and thus the ring is said to be a phase dislocation.[14] The ring's radius, k_V, increases as the value of σ_c decreases, i.e., as the beam becomes less coherent. Unlike in the initial plane, the far-field intensity at the origin is nonzero, $I^{\infty}(0) \neq 0$, unless the beam is coherent. And rather than being singular, the normalized cross correlation at the origin is unity: $\chi^{\infty}(0) = 1$ (except when $\sigma_c \to \infty$). The far-field beam is therefore correlated for $k < k_V$ and anticorrelated for $k > k_V$. From an experimental point of view this ring suggests that black (white) fringes generated by a wave-front folding interferometer will shift to white (black) on either side of the ring.

B. Off-Axis Case, $s\neq 0$, $m=1$

Without loss of generality we may assume that the vortex is displaced along the x axis: $s_x = s$, $s_y = 0$. The far-field MCF may then be written as

$$\Gamma^{\infty}_{m=1}(\mathbf{k}_1, \mathbf{k}_2) = (E_0/\lambda z_d w_0)^2\Big(\int\int [x_1x_2 - s(x_2 + x_1)]T_x\mathrm{d}x_1\mathrm{d}x_2\int\int T_y\mathrm{d}y_1\mathrm{d}y_2 + s^2\int\int T_x\mathrm{d}x_1\mathrm{d}x_2\int\int T_y\mathrm{d}y_1\mathrm{d}y_2 + \int\int T_x\mathrm{d}x_1\mathrm{d}x_2\int\int [y_1y_2 + is(y_2 - y_1)]T_y\mathrm{d}y_1\mathrm{d}y_2 + \int\int x_2T_x\mathrm{d}x_1\mathrm{d}x_2\int\int iy_1T_y\mathrm{d}y_1\mathrm{d}y_2 - \int\int x_1T_x\mathrm{d}x_1\mathrm{d}x_2\int\int iy_2T_y\mathrm{d}y_1\mathrm{d}y_2\Big). \tag{9}$$

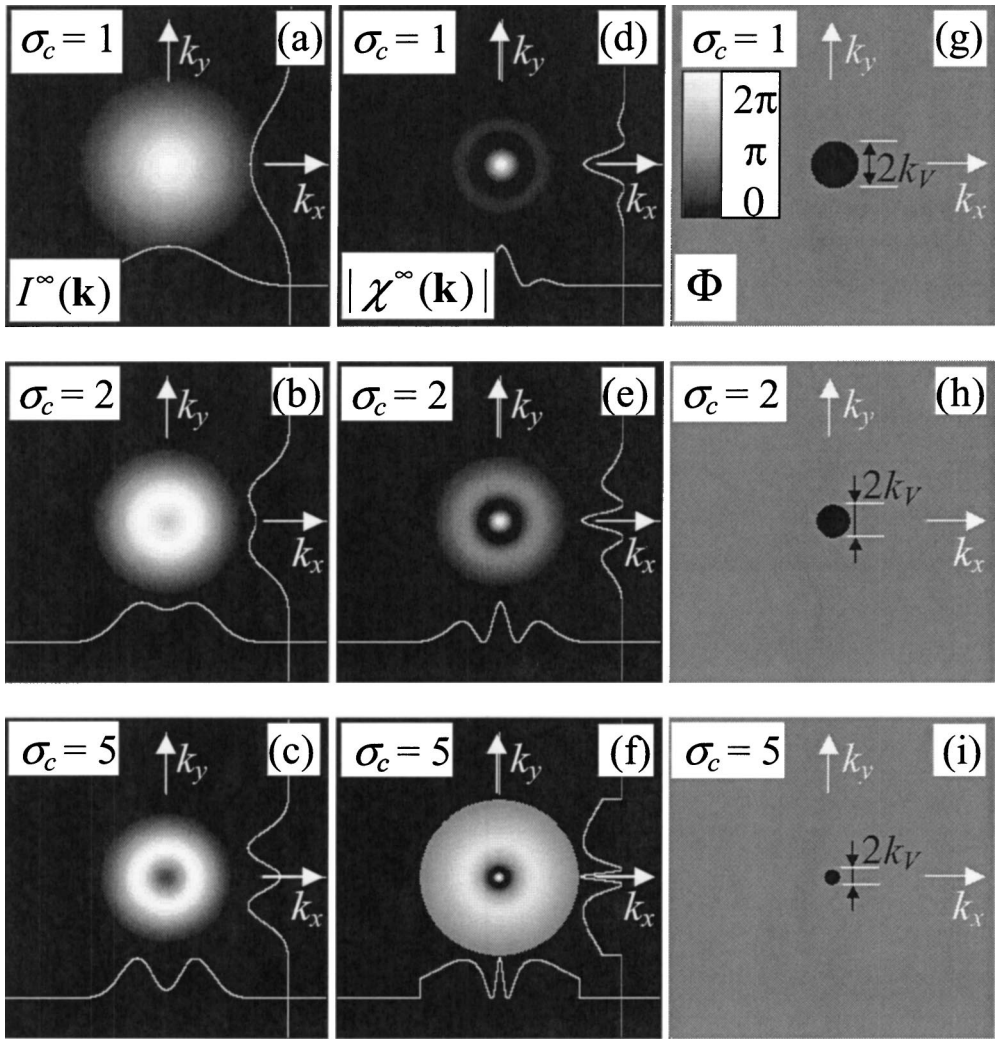

Fig. 3. Numerically calculated far-field distributions of intensity $I^{\infty}(\mathbf{k})$ and normalized cross correlation $\chi^{\infty}(\mathbf{k})$ for an initial on-axis vortex ($s = 0$) of topological charge $m = 1$. Intensity profiles (a)–(c) depict an increasingly distinct vortex core as the relative coherence length, $\sigma_c = l_c/w_0$, increases from low ($\sigma_c = 1$) to medium ($\sigma_c = 2$) to high ($\sigma_c = 5$) coherence. The corresponding magnitudes (d)–(f) and phases (g)–(i) of $\chi^{\infty}(\mathbf{k})$ demonstrate the formation of a ring dislocation of diameter $2k_V$ that persists for arbitrary values of σ_c. When $s = 0$, $\chi^{\infty}(\mathbf{k})$ is real and positive (negative) inside (outside) the dislocation ring. Line plots of values along the k_x and k_y axes are overlaid on the corresponding images as an aid to the eye.

Numerical calculations for the partially coherent case $\sigma_c = l_c/w_0 = 2$ are shown in Fig. 4 for two cases: $s/w_0 = 0.2$ and $s/w_0 = 0.4$. Each intensity profile [Figs. 4(a) and 4(b)] exhibits a diffuse dark core that is translated in a direction that is perpendicular to the initial displacement vector, **s**. One may understand this far-field displacement by considering that each coherent field in our ensemble undergoes a Gouy phase shift on propagating from the near field to the far field. The position of a vortex in a propagating coherent beam is described in Ref. 15.

The corresponding values of $|\chi^{\infty}(\mathbf{k})|$, shown in Figs. 4(c) and 4(d), and of $\Phi(\mathbf{k})$, shown in Figs. 4(e) and 4(f), depict a pair of large-core vortices rather than a ring dislocation [Fig. 3(e)]. The variation of phase near the singularities in Figs. 4(e) and 4(f) indicate topological charges of $M = 1$ at $k_y = k_V$ and $M = -1$ at $k_y = -k_V$. The presence of large-core correlation vortices suggests that large patches of the far-field beam are uncorrelated and may therefore serve as low-coherence light sources. Similarly to the on-axis case, Figs. 4(e) and 4(f) indicate that the beam is anticorrelated ($\Phi = \pi$) for $k \gg k_v$ and correlated ($\Phi = 0,2\pi$) for $k \ll k_v$.

To develop an understanding of the ways in which the initial coherence length affects the far-field MCF we computed the far-field intensity and the normalized cross-correlation function for several values of σ_c. Figure 5 shows these results when $s/w_0 = 0.2$ for low coherence, $\sigma_c = 1$, and high coherence, $\sigma_c = 4$. As expected, the low-coherence intensity profile, Fig. 5(a), reveals no evidence of a vortex core, whereas the core is easily distinguished in the high-coherence case, Fig. 5(b). Comparing the corresponding distributions of $|\chi^{\infty}(\mathbf{k})|$, we can see that the low-coherence profile, Fig. 5(c), is highly localized, whereas the high-coherence profile, Fig. 5(d), is broad. The phase distributions in Figs. 5(e) and 5(f) suggest that the distance between the far-field correlation vortices decreases with increasing values of σ_c.

Figure 6 shows the relation between the far-field dislocations and the initial vortex displacement for three val-

ues of σ_c. For a coherent beam ($\sigma_c \gg 1$) we find that k_V is a linear function of s: $k_V = 2s/w_0^2$. For partially coherent beams we see that $k_v w_0$ always exceeds the coherent value for a given value of s/w_0. For example, the on-axis case ($s = 0$) exhibits a dislocation ring that increases inversely in size with σ_c.[14]

5. CONCLUSIONS

Spatial correlation vortices in a cross-correlation function were analytically and numerically investigated. When a single vortex of topological charge $m = 1$ is present in a partially coherent beam, a pair of oppositely charged

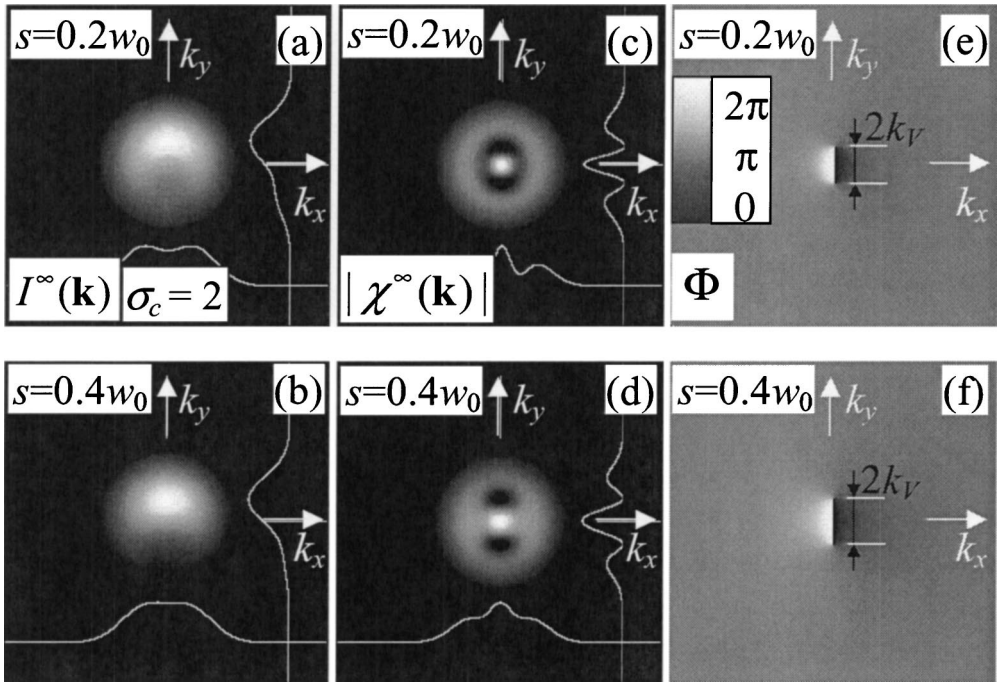

Fig. 4. Numerically calculated far-field distributions of intensity $I^{\infty}(\mathbf{k})$ and normalized cross correlation $\chi^{\infty}(\mathbf{k})$ for an initial off-axis vortex ($s_x \neq 0$, $s_y = 0$) of topological charge $m = 1$ and medium coherence ($\sigma_c = 2$). Intensity profiles depict a diffuse core along the $-k_y$ axis for (a) $s_x/w_0 = 0.2$ and (b) $s_x/w_0 = 0.4$. The magnitudes (c) and (d) and the phases (e) and (f) of $\chi^{\infty}(\mathbf{k})$ reveal a pair of oppositely charged spatial correlation vortices separated by $2k_V$ and that have opposite topological charges.

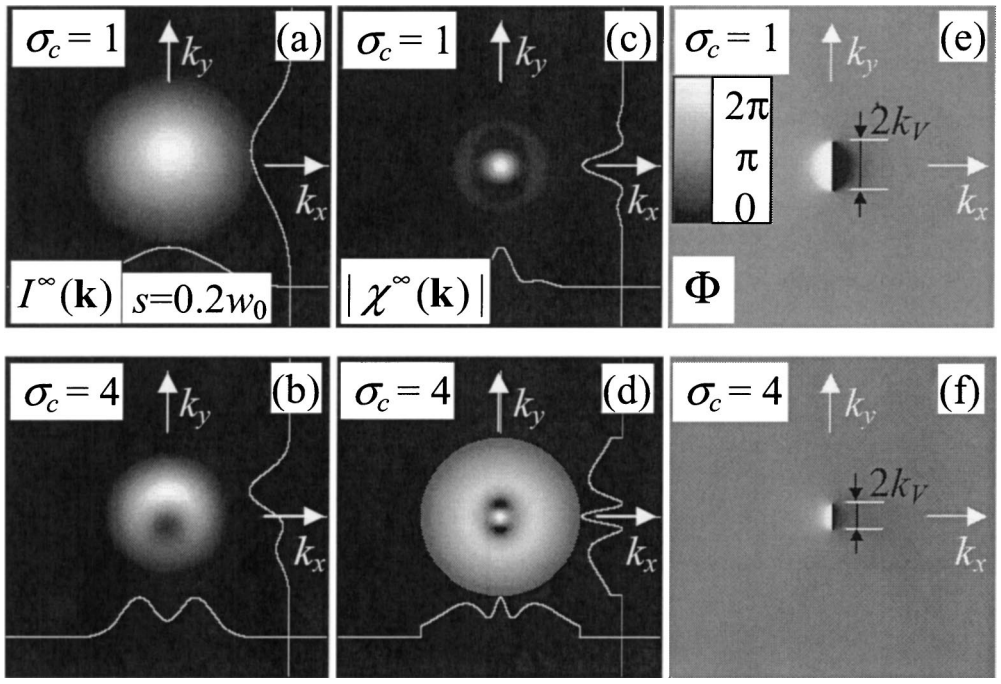

Fig. 5. Same as Figs. 4(a), 4(c), and 4(e) except for the low- ($\sigma_c = 1$) and high- ($\sigma_c = 4$) coherence cases.

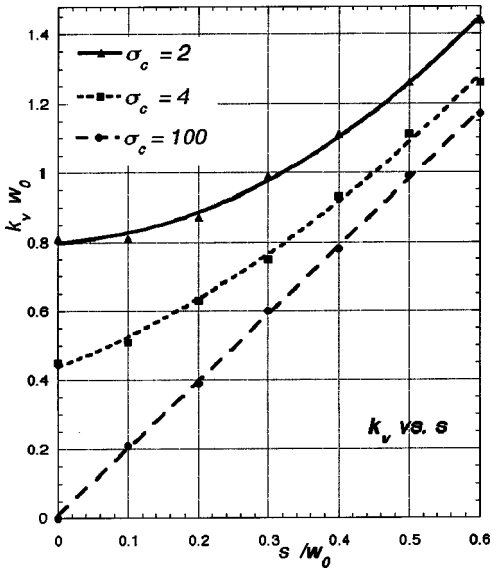

Fig. 6. Plots of radial distance between spatial correlation vortices, k_V, as a function of initial electromagnetic vortex displacement s for three values of initial relative coherence length $\sigma_c = l_c/w_0$. Values along both axes are normalized by the initial beam size, w_0. Numerically calculated values are shown as data marks, and second-order polynomial fits are included to aid the eye.

SCVs (i.e., a dipole) is manifest in both the initial plane and the far-field regions. Those in the initial plane are characterized as point vortices, and they occur at $\mathbf{r} = \pm\mathbf{s}$, where $\mathbf{s}$ is the displacement of the vortex from the beam center. We found large-core SCVs in the far-field region at positions $\pm\mathbf{k}_V$, where $\mathbf{k}_V$ depends on both the initial position and the initial coherence length and the direction of $\mathbf{k}_v$ is perpendicular to $\mathbf{s}$. Having examined only the self- and cross-correlation projections of the four-dimensional mutual coherence function, we have not yet explored the four-dimensional path of the singularities.

ACKNOWLEDGMENT

This study was supported by the U.S. Army Research Office and the state of Arizona.

The e-mail address of G. A. Swartzlander, Jr., is grovers@optics.arizona.edu.

REFERENCES AND NOTES

1. J. F. Nye and M. V. Berry, "Dislocations in wave trains," Proc. R. Soc. London, Ser. A **336**, 165–190 (1974).
2. G. A. Swartzlander, Jr., "Optical vortex filaments," in *Optical Vortices*, M. Vasnetsov and K. Staliunas, eds., Vol. 228 of Horizons in World Physics (Nova Science, Huntington, N.Y., 1999).
3. A. Marathay, *Elements of Optical Coherence Theory* (Wiley, New York, 1982).
4. L. Mandel and E. Wolf, *Optical Coherence and Quantum Optics* (Cambridge U. Press, New York, 1995).
5. Z. Bouchal and J. Perina, "Non-diffracting beams with controlled spatial coherence," J. Mod. Opt. **49**, 1673–1689 (2002).
6. F. Gori, M. Santarsiero, R. Borghi, and S. Vicalvi, "Partially coherent sources with helicoidal modes," J. Mod. Opt. **45**, 539–554 (1998).
7. G. A. Swartzlander, Jr., "Peering into darkness with a vortex spatial filter," Opt. Lett. **26**, 497–499 (2001).
8. D. Palacios, D. Rozas, and G. A. Swartzlander, Jr., "Observed scattering into a dark optical vortex core," Phys. Rev. Lett. **88**, 103902 (2002).
9. H. Gross, "Numerical propagation of partially coherent laser beams through optical systems," Opt. Laser Technol. **29**, 257–260 (1997).
10. H. Schouten, G. Gbur, T. Visser, and E. Wolf, "Phase singularities of the coherence functions in Young's interference pattern," Opt. Lett. **28**, 968–970 (2003).
11. G. Gbur and T. Visser, "Coherence vortices in partially coherent beams," Opt. Commun. **222**, 117–125 (2003).
12. G. Bogatyryova, C. Fel'de, P. Polyanskii, S. Ponomarenko, M. Soskin, and E. Wolf, "Partially coherent vortex beams with a separable phase," Opt. Lett. **28**, 878–880 (2003).
13. I. D. Maleev and G. A. Swartzlander, Jr., "Composite optical vortices," J. Opt. Soc. Am. B **20**, 1169–1176 (2003).
14. D. M. Palacios, I. D. Maleev, A. S. Marathay, and G. A. Swartzlander, Jr., "Spatial correlation singularity of a vortex field," Phys. Rev. Lett. **92**, 143905 (2004).
15. D. Rozas, Z. S. Sacks, and G. A. Swartzlander, Jr., "Experimental observation of fluidlike motion of optical vortices," Phys. Rev. Lett. **79**, 3399–3402 (1997).
16. Z. S. Sacks, D. Rozas, and G. A. Swartzlander, Jr., "Holographic formation of optical votex filaments," J. Opt. Soc. Am. B **15**, 2226–2234 (1998).
17. G. A. Swartzlander, Jr., "Optical vortex solitons," in *Spatial Solitons*, S. Trillo and W. Torruellas, eds. (Springer-Verlag, Berlin, 2001), p. 299.
18. W. Press, S. Teukolsky, W. Vetterling, and B. Flannery, *Numerical Recipes in C++* (Cambridge U. Press, Cambridge, 2002), p. 501.
19. The value of χ may diverge as the intensity vanishes. To prevent this problem we truncate the value of χ when the intensity falls below 2% of the maximum value.